HHS Public Access

Author manuscript

Dev Cell. Author manuscript; available in PMC 2021 July 28.

Published in final edited form as:

Dev Cell. 2019 December 02; 51(5): 575–586.e4. doi:10.1016/j.devcel.2019.10.007.

Prominin2 Drives Ferroptosis Resistance by Stimulating Multivesicular Body/Exosome-Mediated Iron Export

Caitlin W. Brown[1], **John J. Amante**[1], **Peter Chhoy**[1], **Ameer L. Elaimy**[1], **Haibo Liu**[1], **Lihua Julie Zhu**[1], **Christina E. Baer**[2,3], **Scott J. Dixon**[4], **Arthur M. Mercurio**[1,*]

[1]Department of Molecular, Cell and Cancer Biology, University of Massachusetts Medical School, Worcester, MA 01605 USA

[2]Department of Microbiology and Physiological Systems, University of Massachusetts Medical School, Worcester, MA 01605 USA

[3]Sanderson Center for Optical Examination, University of Massachusetts Medical School, Worcester, MA 01605 USA

[4]Department of Biology, Stanford University, Stanford, CA 94305 USA.

Summary

Ferroptosis, regulated cell death characterized by the iron-dependent accumulation of lethal lipid reactive oxygen species, contributes to tissue homeostasis and numerous pathologies, and it may be exploited for therapy. Cells differ in their sensitivity to ferroptosis, however, and a key challenge is to understand mechanisms that contribute to resistance. Using RNA-Seq to identify genes that contribute to ferroptosis resistance, we discovered that pro-ferroptotic stimuli including inhibition of the lipid hydroperoxidase GPX4 and detachment from the extracellular matrix induce expression of prominin2, a pentaspanin protein implicated in regulation of lipid dynamics. Prominin2 facilitates ferroptosis resistance in mammary epithelial and breast carcinoma cells. Mechanistically, prominin2 promotes the formation of ferritin-containing multi-vesicular bodies (MVBs) and exosomes that transport iron out of the cell, inhibiting ferroptosis. These findings reveal that ferroptosis resistance can be driven by a prominin2-MVB/exosome-ferritin pathway and have broad implications for iron homeostasis, intracellular trafficking and cancer.

Introduction

Ferroptosis is a regulated form of non-apoptotic cell death characterized by the iron-dependent accumulation of lethal lipid reactive oxygen species (ROS) (Dixon et al., 2012; Yang et al., 2016; Yang and Stockwell, 2016). This process can contribute to pathological cell death in brain, kidney, heart and other tissues (Do Van et al., 2016; Fang et al., 2019; Friedmann Angeli et al., 2014; Hangauer MJ, 2017; Hirschhorn and Stockwell, 2019). There

*Lead Contact: Arthur M. Mercurio, Department of Molecular, Cell and Cancer Biology, University of Massachusetts Medical School Worcester, MA 01605; arthur.mercurio@umassmed.edu; Tel. (508) 856-8676; Fax (508) 856-1310.

Author Contributions: CWB and AMM conceived the study and designed experiments, and wrote the manuscript. CWB performed most of the experiments. JJA, PC and ALE contributed to specific experiments. HL and LJZ performed bioinformatics analysis of RNA sequencing data. CEB assisted with immunofluorescence imaging. SJD provided critical input into the study and manuscript.

Declaration of Interests: The authors declare no competing interests.

is also interest in understanding the role of ferroptosis in cancer, and potentially exploiting this mechanism therapeutically (Dixon, 2019). Interestingly, ferroptosis sensitivity varies substantially among cancer cells from distinct tissue lineages that express certain tumor suppressors, or have acquired unique cell drug-tolerant or de-differentiated cell states (Hangauer MJ et al., 2017; Jiang et al., 2015; Tsoi et al., 2018; Viswanathan VS et al., 2017; Yang et al., 2014; Zhang et al., 2019). At the molecular level, mechanisms that can account for the observed variation in ferroptosis sensitivity between cells remain largely elusive.

Ferroptosis can be initiated by a number of stimuli that disrupt intracellular gluthione-mediated antioxidant systems or directly overload the cell with iron (Stockwell et al., 2017). For example, it is possible to induce ferroptosis by depriving cells of the thiol-containing amino acid cystine (the disulfide of cysteine), a key glutathione precursor, or by directly inhibiting the reduced glutathione (GSH)-dependent phospholipid hydroperoxiodase glutathione peroxidase 4 (GPX4) (Dixon et al., 2012; Yang et al., 2014). GPX4 catalyzes the reduction of reactive lipid hydroperoxides to non-reactive lipid alcohols. This reaction is essential to prevent a buildup of lipid hydroperoxides, which can participate in Fenton chemistry reactions when free iron is present that lead to the generation of toxic lipid alkoxy radicals and subsequently other reactive lipid breakdown products (Dixon, 2019). The execution of ferroptosis, therefore, relies on the combined presence of oxidizable lipids (e.g. polyunsaturated phospholipids) and free iron which, in the absence of sufficient GPX4-mediated lipid peroxide detoxification, result in oxidative destruction of the plasma membrane and other internal organelle membranes (Agmon et al., 2018; Magtanong et al., 2019). Physiological stress such as detachment of cells from the extracellular matrix can increase ROS and is sufficient to trigger ferroptosis if GPX4 activity is inhibited (Brown CW et al., 2017).

Iron is essential for cell growth but it can also promote toxic ROS formation, as occurs during ferroptosis (Torti SV et al., 2018). How intracellular iron homeostasis contributes to ferroptosis sensitivity is only partially understood. Iron can be taken into cells via the transferrin/transferrin receptor system, and genetic silencing of the transferrin receptor partially inhibits ferroptosis (Gao et al., 2016; Yang and Stockwell, 2008). NCOA4-mediated, lysosomal-dependent degradation of the iron storage protein ferritin contributes to the pool of free intracellular iron and thereby promotes ferroptosis; genetic depletion of *NCOA4* or chemical inhibition of lysosomal acidification both attenuate ferroptosis (Gao et al., 2016; Hou et al., 2016; Torii et al., 2016). Furthermore, manipulation of ferroportin-mediated iron export can alter ferroptosis sensitivity, with reduced ferroportin expression leading to less iron export and increased ferroptosis sensitivity (Geng N et al., 2018; Ma et al., 2016). Thus, the modulation of intracellular free iron levels by the cellular iron homeostatic network emerges as a key regulator of ferroptosis sensitivity. Interestingly, intracellular free iron levels can vary between cancer cells and cancer cell states (e.g. in metastatic versus non-metastatic cells), which might be expected to contribute to differences in ferroptosis sensitivity (Geng N et al., 2018). There is also some evidence that iron levels may be dynamically regulated within the cell in response to ferroptosis-inducing conditions, suggesting that uncharacterized regulatory mechanisms may alter intracellular iron, possibly in an attempt to negatively regulate the onset of ferroptosis (Ma et al., 2016).

In this study, we used an unbiased approach to investigate how mammary epithelial and breast carcinoma cells survive in response to pharmacological and physiological ferroptotic stress. We observed that cells can resist the onset of ferroptosis by dynamically upregulating an unprecedented iron export pathway involving multi-vesicular body (MVB)/exosome trafficking of ferritin and iron out of the cell. This process limits the intracellular accumulation of free iron and inhibits the onset of ferroptosis. By contrast, inactivation of this program, either normally or following chemical or genetic inhibition of key steps of this process, substantially increases ferroptosis sensitivity. These findings pinpoint a novel mechanism that leads to variation in ferroptosis sensitivity and suggest that dynamic MVB/exosome-mediated iron export may be a homeostatic mechanism acting to restrict the initiation of ferroptosis, thereby preventing cell death under conditions of sub-lethal stress exposure.

Results

Prominin2 is induced by ferroptotic stress and promotes resistance to ferroptotic cell death:

To gain insight into mechanisms that promote ferroptosis resistance, we exploited our recent finding that detachment of certain cells from the extracellular matrix (ECM) is a pro-ferroptotic stress (Brown CW et al., 2018; Brown CW et al., 2017). We reasoned that cells that can survive under detached conditions may do so by upregulating a protective gene expression program that prevents cell death. To identify such genes, we compared mRNA expression in adherent and ECM-detached MCF10A immortalized breast epithelial cells by RNA-sequencing (GSE115059). *PROM2*, which encodes the pentaspanin protein prominin2, captured our attention because its expression was significantly increased in ECM-detached cells compared to adherent cells. Also, it is thought to have a role in lipid dynamics and membrane organization, processes that could be relevant for ferroptosis resistance (Doll S et al., 2017; Florek M et al., 2007; Jászai J et al., 2010; Singh RD et al., 2013). We confirmed that prominin2 was rapidly upregulated in MCF10A cells in response to ECM detachment at the protein and mRNA level (Figures 1A,B). Increased PROM2 was also observed in detached versus adherent Hs578t breast cancer cells (Figure 1B). Silencing of prominin2 expression in both MCF10A and Hs578t cells resulted in a significant loss of viability in ECM-detached conditions (Figures 1B,C). Cell viability under these conditions was rescued by co-treatment with a specific inhibitor of ferroptosis, ferrostatin-1 (Dixon et al., 2012), but not the pan-caspase inhibitor ZVAD-fmk (Figure 1C). These data indicate that failure to upregulate PROM2 upon ECM detachment can result in the induction of ferroptosis.

We next investigated whether pharmacological inhibition of GPX4 altered prominin2 expression and impacted ferroptosis in adherent cells. MCF10A and Hs578t cells were treated with RSL3, a covalent GPX4 inhibitor (Yang et al., 2014), for 2 hrs resulting in increased prominin2 mRNA and protein expression in both cell lines (Figures 1D,E). This effect was not a generic response to ROS stress because culturing with H_2O_2 did not increase prominin2 expression (Figure S1A). Moreover, expression of a related family member, prominin1 (CD133), was not altered significantly by RSL3, substantiating the specificity of the ferroptotic effect for prominin2 (Figure S1A). Unlike MCF10A and Hs578t

cells, RSL3 did not induce prominin2 in MDA-MB-231 cells, another breast cancer cell line (Figures 1D,E). We observed that the induction of prominin2 expression correlated with resistance to ferroptosis induced by GPX4 inhibition. MCF10A and Hs578t cells were resistant to RSL3-induced cell death at concentrations up to 2.5 μM, while MDA-MB-231 cells were killed by RSL3 concentrations as low as 0.5 μM (Figure 1F).

Given the above results, we assessed whether prominin2 was necessary for resistance to ferroptosis. For this purpose, we silenced prominin2 expression in MCF10A and Hs578t cells (Figure S1B) and examined the sensitivity of these cells to ferroptosis compared to control cells. Here, we tested the covalent GPX4 inhibitors RSL3, ML210 (Weïwer M et al., 2012), the indirect GPX4 inhibitor FIN56 (Shimada K et al., 2016) and the GSH-depleting agent erastin, which reduces GPX4 activity indirectly by preventing the synthesis of its key cofactor (Dixon et al., 2012). Control MCF10A cells were more resistant to these compounds than Hs578t cells (Figures 2A,B). Nonetheless, a significant increase in sensitivity to all four compounds was observed in prominin2 knock-down cells compared to control cells for both cell lines (Figures 2A,B, A,B). Loss of cell viability in prominin2-depleted cells was completely rescued by ferrostatin-1, indicating that the greater sensitivity of prominin2-silenced cells was not caused by the induction of an alternative mode of cell death (Figure 2C). Given the results obtained with genetic silencing, we next tested whether overexpression of prominin2 was sufficient to inhibit ferroptosis. Indeed, exogenous prominin2 expression in MDA-MB-231 cells was sufficient to inhibit cell death in response to RSL3, ML210, FIN56 and erastin (Figures 2D, S2C,D). Thus, prominin2 expression promotes resistance to ferroptosis. Subsequent experiments were performed using RSL3 as a prototypic GPX4 inhibitor.

Prominin2 promotes the formation of multivesicular bodies and exosomes: To gain insight into how prominin2 may promote ferroptosis resistance, we assessed its subcellular localization following GPX4 inhibition. Immunofluorescence microscopy revealed that prominin2 localizes in discrete cytoplasmic puncta in response to GPX4 inhibition by RSL3 (Figures 3A, S3A). As determined using organelle-specific markers, these puncta did not co-localize with early endosomes (Rab5A), peroxisomes (catalase), caveolae (phospho-Caveolin-1), autophagosomes (LC3) or mitochondria (Mitotracker) (Figure S3B). By contrast, a striking co-localization was observed between prominin2 and TSG101, a marker of multivesicular bodies (MVBs) (Razi M et al., 2006) (Figures 3A, S3A). MVBs are late endosomes containing cargo within their lumen bound in intraluminal vesicles (ILVs) (Felder S et al., 1990; Gruenberg J et al., 1995). The cargo can be sorted for degradation in lysosomes or released into the extracellular space as exosomes (Futter CE et al., 1996; Hart PD et al., 1991). The co-localization of prominin2 and TSG101 was evident as early as 30 min following the inhibition of GPX4 and this co-localization was most prominent in the perinuclear region (Figure 3B, S4A). At later times (1.5 to 2 hrs), this co-localization was evident throughout the cytoplasm. We also observed that prominin2 exhibited some co-localization with the lysosomal marker LAMP1 (Cella N et al., 1996) (Figure S3C), which is expected given that some MVBs are trafficked to lysosomes (Futter CE et al., 1996; Razi M et al., 2006). However, we discounted a role for lysosomes in ferroptosis resistance under these conditions based on the observation that NH_4Cl treatment,

which inhibits lysosome function (Hart PD et al., 1991), had no effect on the survival of either control or prominin2-depleted cells following GPX4 inhibition (Figure S3D).

The above results prompted us to assess whether prominin-2 promotes MVB formation in response to GPX4 inhibition. RSL3-treated MCF10A and Hs578t cells contained more TSG101-positive structures than vehicle control-treated cells, indicating that GPX4 inhibition induces MVB formation (Figures 3A,B, S4A). Prominin2 localization to MVBs in RSL3-treated MCF10A and Hs578t cells was confirmed by co-localization with Alix and CD9 (Figures S4B, C). We then evaluated whether the formation of these structures is dependent on prominin2 using transmission electron microscopy (TEM). Indeed, RSL3-treated MCF10A cells contained significantly more MVBs per cell than control cells, an effect that was not observed in prominin2-silenced cells (Figure 3C). Notably, this RSL3-stimulated increase in MVBs was rapid (within 2 hr). Immunofluorescence microscopy also revealed a reduction in TSG101-positive puncta in prominin2-depleted MCF10A and Hs578t cells compared to control cells (Figures 3D,E, S5A,B). Conversely, exogenous prominin2 expression in MDA-MB-231 cells increased the number of TSG101-positive structures and, as noted above, reduced ferroptosis sensitivity (Figures 3F, S5C). Consistent with a causal role for MVBs in ferroptosis resistance, diminishing TSG101 expression increased the sensitivity of MCF10A and Hs578t cells to RSL3-induced cell death (Figures 4A,B, S6A) and this death was rescued with ferrostatin-1 (Figure 4C). These data indicate that GPX4 inhibition stimulates prominin2 expression and prominin2-dependent MVB formation, which promote ferroptosis resistance.

MVBs can fuse with the plasma membrane and release intraluminal vesicles (ILVs) as exosomes (Harding C et al., 1984; Pan BT et al., 1985). Indeed, we observed distinct ILVs in MVBs consistent with the size of exosomes (~80nm) (Raposo and Stoorvogel, 2013) in RSL3-treated cells (Figure 3C). To assess the impact of GPX4 inhibition on exosome formation, exosomes were harvested by ultracentrifugation from control (DMSO) and RSL3-treated MCF10A and Hs578t cells. The presence of an exosome fraction was confirmed by TEM (Figure S6B). GPX4 inhibition increased exosome formation as evidenced by the fact that a significant amount of protein was present in the exosome preparation of RSL3-treated cells (Figure 4D). In contrast, exosomal protein in control cells was not detected in this experiment (data not shown). Analysis of these exosomes by immunoblotting revealed that they contained prominin2, CD63 and TSG101 providing evidence that they were generated by prominin2-dependent MVB formation (Figure 4D). Importantly, they did not contain GM130, a Golgi marker, indicating that their isolation was not contaminated with other cell membranes. To test whether exosome release was essential for resistance to GPX4 inhibition, we used the sphingomyelinase inhibitor GW4869 and found that inhibition of exosome release increased the sensitivity of control MCF10A and Hs578t cells to RSL3 but it did not significantly impact the viability of prominin2-depleted cells (Figure 4E).

Ferroptosis resistance is facilitated by MVB/exosome iron transport: Our results indicated that prominin2-mediated MVB and exosome formation promote ferroptosis resistance. We hypothesized that this resistance mechanism involved MVBs and exosome-mediated export of a factor that would otherwise promote ferroptosis. Given that the iron

storage protein ferritin can be secreted from cells in exosomes (Truman-Rosentsvit M et al., 2018), we reasoned that MVB/exosome-mediated ferritin export inhibits ferroptosis. In support of this hypothesis, we observed that ferritin co-localized with prominin2 in RSL3-treated MCF10A and Hs578t cells, but not in vehicle control (DMSO)-treated cells (Figure 5A). We also identified ferritin protein in exosomes harvested from these cells (Figure 5B). These exosomes contained iron as detected by inductively coupled plasma mass spectrometry (ICP-MS) (3400 ng per exosome collection), further supporting our hypothesis. MDA-MB-231 cells do not increase ferritin expression following GPX4 inhibition. However, the expression of exogenous prominin2 induced a more punctate pattern of ferritin localization in RSL3-treated compared to control cells (Figure 5C). An alternative explanation for our findings was that prominin2 enhanced the membrane localization of the iron exporter ferroportin, which has been shown to play a role in ferroptosis sensitivity (Geng N, 2018). However this did not appear to be the case because prominin2 did not co-localize with ferroportin (SLC40A1) (Figure S6C).

A causal role for ferritin in ferroptosis resistance is supported by the finding that knock-down of both the ferritin heavy chain (*FTH1*) and light chain (*FTL*) increased cell death triggered by GPX4 inhibition in both MCF10A and Hs578t cells (Figures 5D,E, S6D). Importantly, this death was rescued by either ferrostatin-1 or the iron chelator deferoxamine (DFO), providing evidence for its ferroptotic nature (Figure 5F).

Our data suggested that GPX4 inhibition stimulates the formation of MVBs containing ferritin and that these structures transport iron out of the cell. To test this hypothesis, we quantified the free iron concentration in control and RSL3-treated MCF10A and Hs578t cells and observed no significant difference between these two groups (Figure 6A). However, we observed an increase in the concentration of free iron following RSL3 treatment when either prominin2 or both FTH1 and FTL were silenced (Figures 6A,B, S6D). Additional evidence for prominin2 regulation of iron levels was obtained by quantifying free iron in control and prominin2-expressing MDA-MB-231 cells in response to GPX4 inhibition. Prominin2 expression in these cells prevented the increase in iron in response to RSL3 that was observed in control cells (Figure 6C). Also, disabling the MVB pathway by decreasing expression of TSG101 significantly increased the concentration of free intracellular iron following GPX4 inhibition (Figure 6D). These results indicate that blocking MVB/exosome-mediated ferritin export results in an accumulation of intracellular iron upon GPX4 inhibition.

ECM-detached cells resist ferroptosis by prominin2-mediated MVB/exosome formation: Based on the observation that ECM-detachment is a ferroptotic stress that induces prominin2 expression (Figure 1B), we investigated whether prominin2 promotes MVB formation and iron transport in ECM-detached cells. Indeed, cell death in ECM-detached, prominin2-depleted MCF10A and Hs578t cells was rescued by the iron chelator deferoxamine, consistent with a defect in iron export promoting cell death (Figure 7A). Also, ECM detachment increased the concentration of free iron in prominin2-depleted compared to control cells, an effect that was most noticeable 2 hrs post-detachment, which is coincident with the onset of ferroptosis (Figure 7B). Similar to RSL3-treated adherent cells, ECM detachment increased the frequency of MVBs based on TEM analysis and this

increase was dependent on prominin2 (Figure 7C). Exosome release is indicated by the fusion of an MVB with the plasma membrane (Figure 7C). Co-localization of prominin2 and TSG101 was also evident in ECM-detached MCF10A and Hs578t cells (Figures 7D), similar to the co-localization seen in adherent, RSL3-treated cells (Figure 3A). These results indicate that physiological ferroptotic stress can be evaded by the prominin2/MVB iron export pathway.

Discussion

We have uncovered a cell biological mechanism of ferroptosis resistance that has broad implications for understanding how cells respond to pro-ferroptotic conditions. The critical component of this mechanism is the pentaspanin protein prominin2, whose expression can be increased by pharmacological and physiological triggers of ferroptosis. The induction of prominin2 expression in response to ferroptotic stress promotes the formation of MVBs and exosomes that function to transport iron out of the cell and, consequently, impede ferroptosis. The existence of this mechanism suggests that cells have evolved a regulated means to evade ferroptosis that involves limiting the intracellular concentration of this potentially toxic metal in times of stress. Cells that cannot induce prominin2 and export ferritin are therefore highly sensitive to the induction of ferroptosis.

Our finding that prominin2 is at the nexus of a ferroptosis resistance mechanism heightens interest in this protein. While little is known about prominin2, there is evidence that it can localize to microvilli, cilium and other protrusions from the apical and basolateral membranes in epithelial cells (Florek M et al., 2007; Jászai J et al., 2010; Singh RD et al., 2013) and regulate lipid microdomains by binding cholesterol (Florek M et al., 2007). In contrast to these studies, however, we observed that prominin2 is not localized on the plasma membrane but rather intracellularly in MVBs. Mechanistically, how prominin2 stimulates MVB formation is an important topic for future investigation. One possibility is that prominin2 regulates cholesterol levels in late endosomes, a process that appears to be critical for MVB formation (Kobuna et al., 2010).

Free iron is essential for the execution of ferroptosis (Dixon et al., 2012; Dixon et al., 2014), and an increase in iron import combined with reduced ferritin storage capacity is a characteristic of erastin-sensitive cells (Torti SV et al., 2018; Yang and Stockwell, 2008). The concept that intracellular iron levels and ferroptosis sensitivity may be modulated on short (<2 h) timescales through the export of ferritin from the cell via an MVB/exosome pathway had not been considered previously. Speculatively, reducing ferroptosis sensitivity may be a physiological role for the process of MVB-mediated ferritin export observed previously (Truman-Rosentsvit M et al., 2018). Our results imply that cytosolic iron increases in response to GPX4 inhibition or ECM detachment, but that this iron can be captured, incorporated into MVBs, and exported from the cell in exosomes if prominin2 expression is sufficient. It could be argued that the uptake of the released, ferritin-containing exosomes by neighboring cells diminishes the overall decrease in intracellular iron. However, our finding that exosomes accumulate detectably in the medium suggests that the rate of exosome release from cells far exceeds their rate of uptake. In this direction, it is

possible that a cell with partially oxidized membranes as a result of GPX4 inhibition is defective in exosome uptake.

This mechanism of prominin2-mediated ferroptosis resistance has potential implications for efforts that seek to induce ferroptosis as a mode of anti-cancer therapy. For example, inhibiting GPX4 activity can selectively kill certain tumor cells via ferroptosis (Viswanathan VS et al., 2017; Yang et al., 2014). Given that cells can acquire resistance to GPX4 inhibition by inducing prominin2, strategies that simultaneousy block prominin2 expression or function may enhance sensitivity to GPX4 inhibitors. Indeed, analysis of the Broad Institute Cancer Therapeutics Response Portal resource indicates that high levels of prominin2 expression are significantly correlated with resistance to the GPX4 inhibitor ML210 across hundreds of cancer cells lines (https://portals.broadinstitute.org/ctrp/?featureName=PROM2). Given that prominin2 expression is correlated with poor clinical outcomes in several cancers (Saha et al., 2019), prominin2-mediated MVB formation and iron export may also be relevant to the emerging role of ferroptosis in tumor suppression (Jiang et al., 2015).

STAR Methods:

Contact for Reagent and Resource Sharing

Further information and requests for resources and reagents should be directed to and will be fulfilled by the Lead Contact, Arthur Mercurio (arthur.mercurio@umassmed.edu).

Experimental Model and Subject Details

Cell Lines: MCF10A cells were obtained from the Barbara Ann Karmanos Cancer Institute. Hs578T cells were provided by Dr. Dohoon Kim (UMASS Medical School). MDA-MB-231 cells were obtained from the American Type Culture Collection. All cells were checked quarterly for mycoplasma and authenticated using the University of Arizona Genetics Core.

Methods Details

Cell-based assays: Assays to assess survival in response to matrix detachment were performed as described (Brown CW, 2017). To assay survival in response to GPX4 inhibition, adherent cells in 96 well plates (1.0×10^4 per well) were treated with either DMSO, RSL3, ML210, FIN56 or erastin for 24 hrs with and without ferrostatin-1 or DFO. Subsequently, cells were fixed in 4% paraformaldehyde, stained with crystal violet and read on a microplate reader at absorbance 595. Absorbances were normalized to DMSO.

Biochemical experiments: Immunoblotting and qPCR were performed as described (Brown CW et al., 2017). Sequences for primers used were as follows: 18s Forward 5'-AACCCGTTGAACCCCATT-3', Reverse 5'-CCATCCAATCGGTAGTAGCG-3', PROM2 Forward 5'- GCTCAGGAACCCAAACCTGT-3', Reverse 5'-GGCAGGCCATACATCCTTCT-3', PROM1 Forward 5'-AGTCGGAAACTGGCAGATAGC-3', Reverse 5'- GGTAGTGTTGTACTGGGCCAAT-3'.

Total free iron was quantified using the Iron Assay Kit per manufacturer's specifications. Briefly, adherent cells in 10 cm plates (1.0×10^6/well) were treated with either DMSO or RSL3 for 2 hrs, lysed and supernatant was reduced using the provided iron reducer before the mixture was reacted with an iron probe. Plates were read at 595 nm and total iron concentration was obtained using an iron standard curve.

Molecular biology experiments—siRNA-mediated silencing of gene expression was performed with Lipofectamine 3000 per the manufacturer's guidelines using control, prominin2, *TSG101*, or *FTH1* siRNAs. To express prominin2 in MDA-MB-231 cells, a pCMV-prominin2 expression vector was obtained from VectorBuilder. Cells were transfected with this plasmid and a control plasmid using Lipofectamine 3000 and selected for prominin2 expression with G418 (0.5 μg/mL) for ten days.

Immunofluorescence microscopy: For adherent cells, 8 well chamber slides were coated with 1 μg/mL laminin. Cells (5.0×10^4 per well) were plated overnight and then treated for two hours with either DMSO or RSL3, fixed in 4% paraformaldehyde and permeabilized in 0.1% Triton. Slides were blocked in 0.5% BSA, incubated in antibody overnight at 4ºC, washed in PBS and incubated in secondary antibody for 1 hr at room temperature. Slides were washed and mounted in Vectashield with DAPI. For ECM-detached experiments, cells were trypsinized and plated (5.0×10^5 per well) in 60 mm low-adherent plates for two hr, collected and spun down prior to being fixed and stained as described above. Slides were imaged on a Zeiss or a Nikon A-1 confocal microscope.

Exosome isolation: Cells were cultured for 24 hrs in their respective media containing extracellular vesicle (EV) free serum and treated with RSL3 for 24 hours. Culture supernatants were centrifuged at 4°C at 1000 RPM for 5 min, 3000 RPM for 10 min, 4000 RPM for 30 min prior to ultracentrifugation at 22,000 RPM for 140 min at 4°C. Pellets were resuspended in cold PBS and centrifuged again under the same conditions. For immunoblotting, pellets were lysed in RIPA buffer, centrifuged at 10,000 RPM for 15 min and protein concentration was determined by Bradford Assay. For TEM, PBS was removed and 20 μL of the exosome preparation was fixed and processed. For ICP-mass spec, exosome-containing pellet was resuspended in 0.5 mL PBS and centrifuged in a speed-vac at 45°C. Samples were sent to the UMASS Mass Spectrometry Core where they were digested in 100 μL HNO_3, heated to 65°C for 20 min and diluted to 2 mL with ddH_2O before analysis.

Transmission Electron Microscopy: Adherent siControl and siProminin2 cells were treated with DMSO or RSL3 (5μM) for two hr. ECM-detached siControl and siProminin2 cells were maintained for 2 hrs in low-adherence plates. All cells were fixed by adding 2.5% glutaraldehyde (v/v) in 0.1 M Na cacodylate buffer (pH 7.2) and processed for TEM. The samples were examined on a FEI Tecnai 12 BT transmission electron microscope using 100Kv accelerating voltage. Images were captured using a Gatan TEM CCD camera.

Statistics and reproducibility: Statistical comparison between only two groups were done with the unpaired Student's t test. Multiple group comparisons were completed using one-way analysis of variance (ANOVA). Statistical tests were carried out using GraphPad

Prism version 8.0 and a P value of less than 0.05 was considered significant. The bars in graphs represent means ± SEM. *, P < 0.05; **, P < 0.01; ***, P < 0.005. Three independent experiments were performed for each experiment except for transmission electron microscopy experiments in Figures 3C and 7C which were performed once.

Supplementary Material

Refer to Web version on PubMed Central for supplementary material.

Acknowledgments:

This work was supported by DOD Grant W81XWH-17-1-0009 and NIH Grant CA218085 (AMM), ACS Grant 130451-PF-17-105-01-CSM (CWB) and NIH grant 1R01GM122923 (SJD). The Electron Microscopy Core Facility is funded in part by NIH Research equipment grants and by UMMS Office of Research. We thank Dr. Suzy Torti for helpful discussions.

References

Agmon E, Solon J, Bassereau P, and Stockwell BR (2018). Modeling the effects of lipid peroxidation during ferroptosis on membrane properties. Scientific reports 8, 5155. [PubMed: 29581451]

Brown C, Amante JJ, Mercurio AM (2018). Cell clustering mediated by the adhesion protein PVRL4 is necessary for α6β4 integrin-promoted ferroptosis resistance in matrix-detached cells. The Journal of biological chemistry 293, 12741–12748. [PubMed: 29934307]

Brown CW AJ, Goel HL, Mercurio AM (2017). The α6β4 integrin promotes resistance to ferroptosis. The Journal of cell biology 216, 4287–4297. [PubMed: 28972104]

Cella N C-UR, Montes GS, Hynes NE, Chammas R. (1996). The lysosomal-associated membrane protein LAMP-1 is a novel differentiation marker for HC11 mouse mammary epithelial cells. Differentiation 61, 113–120. [PubMed: 8983177]

Dixon S.a.S., BR (2019). The Hallmarks of Ferroptosis. Annu Rev Cancer Biol 3, 35–54.

Dixon SJ, Lemberg KM, Lamprecht MR, Skouta R, Zaitsev EM, Gleason CE, Patel DN, Bauer AJ, Cantley AM, Yang WS, et al. (2012). Ferroptosis: an iron-dependent form of nonapoptotic cell death. Cell 149, 1060–1072. [PubMed: 22632970]

Dixon SJ, Patel DN, Welsch M, Skouta R, Lee ED, Hayano M, Thomas AG, Gleason CE, Tatonetti NP, Slusher BS, et al. (2014). Pharmacological inhibition of cystine– glutamate exchange induces endoplasmic reticulum stress and ferroptosis. eLife 3.

Do Van B, Gouel F, Jonneaux A, Timmerman K, Gelé P, Pétrault M, Bastide M, Laloux C, Moreau C, Bordet R, et al. (2016). Ferroptosis, a newly characterized form of cell death in Parkinson's disease that is regulated by PKC. Neurobiology of Disease 94, 169–178. [PubMed: 27189756]

Doll S, P. B, Tyurina YY, Panzilius E, Kobayashi S, Ingold I, Irmler M, Beckers J, Aichler M, Walch A, Prokisch H, Trümbach D, Mao G, Qu F, Bayir H, Füllekrug J, Scheel CH, Wurst W, Schick JA, Kagan VE, Angeli JP, Conrad M. (2017). ACSL4 dictates ferroptosis sensitivity by shaping cellular lipid composition. Nature chemical biology 13, 91–98. [PubMed: 27842070]

Fang X, Wang H, Han D, Xie E, Yang X, Wei J, Gu S, Gao F, Zhu N, Yin X, et al. (2019). Ferroptosis as a target for protection against cardiomyopathy. Proc Natl Acad Sci U S A 116, 2672–2680. [PubMed: 30692261]

Felder S MK, Moehren G, Ullrich A, Schlessinger J, Hopkins CR. (1990). Kinase activity controls the sorting of the epidermal growth factor receptor within the multivesicular body. Cell 61, 623–634. [PubMed: 2344614]

Florek M, B N, Janich P, Wilsch-Braeuninger M, Fargeas CA, Marzesco AM, Ehninger G, Thiele C, Huttner WB, Corbeil D (2007). Prominin-2 is a cholesterol-binding protein associated with apical and basolateral plasmalemmal protrusions in polarized epithelial cells and released into urine. Cell and tissue research 328, 31–47. [PubMed: 17109118]

Friedmann Angeli JP, Schneider M, Proneth B, Tyurina YY, Tyurin VA, Hammond VJ, Herbach N, Aichler M, Walch A, Eggenhofer E, et al. (2014). Inactivation of the ferroptosis regulator Gpx4 triggers acute renal failure in mice. Nature cell biology 16, 1180–1191. [PubMed: 25402683]

Futter CE, P A, LJ Hewlett, Hopkins CR. (1996). Multivesicular endosomes containing internalized EGF-EGF receptor complexes mature and then fuse directly with lysosomes. The Journal of cell biology 132, 1011–1023. [PubMed: 8601581]

Gao M, Monian P, Pan Q, Zhang W, Xiang J, and Jiang X. (2016). Ferroptosis is an autophagic cell death process. Cell Res 26, 1021–1032. [PubMed: 27514700]

Geng N, S B, Li SL, Zhong ZY, Li YC, Xua WL, Zhou H, Cai JH. (2018). Knockdown of ferroportin accelerates erastin-induced ferroptosis in neuroblastoma cells. Eur Rev Med Pharmacol Sci 22, 3826–3836. [PubMed: 29949159]

Gruenberg J MF (1995). Membrane transport in the endocytic pathway. Current opinion in cell biology 7, 552–563. [PubMed: 7495576]

Hangauer MJ, V V, Ryan MJ, Bole D, Eaton JK, Matov A, Galeas J, Dhruv HD, Berens ME, Schreiber SL, McCormick F, McManus MT. (2017). Drug-tolerant persister cancer cells are vulnerable to GPX4 inhibition. Nature 551, 247–250. [PubMed: 29088702]

Harding C HJ, Stahl P. (1984). Endocytosis and intracellular processing of transferrin and colloidal gold-transferrin in rat reticulocytes: demonstration of a pathway for receptor shedding. Eur J Cell Biol 35, 256–263. [PubMed: 6151502]

Hart PD YM (1991). Ammonium chloride, an inhibitor of phagosome-lysosome fusion in macrophages, concurrently induces phagosome-endosome fusion, and opens a novel pathway: studies of a pathogenic mycobacterium and a nonpathogenic yeast. J Exp Med 174, 881–889. [PubMed: 1919441]

Hirschhorn T, and Stockwell BR (2019). The development of the concept of ferroptosis. Free radical biology & medicine 133, 130–143. [PubMed: 30268886]

Hou W, Xie Y, Song X, Sun X, Lotze MT, Zeh HJ 3rd, Kang R, and Tang D. (2016). Autophagy promotes ferroptosis by degradation of ferritin. Autophagy 12, 1425–1428. [PubMed: 27245739]

Jászai J, F L, Fargeas CA, Janich P, Haase M, Huttner WB, Corbeil D. (2010). Prominin-2 is a novel marker of distal tubules and collecting ducts of the human and murine kidney. Histochem Cell Biol 133, 527–539. [PubMed: 20333396]

Jiang L, Kon N, Li T, Wang SJ, Su T, Hibshoosh H, Baer R, and Gu W. (2015). Ferroptosis as a p53-mediated activity during tumour suppression. Nature 520, 57–62. [PubMed: 25799988]

Kobuna H, Inoue T, Shibata M, Gengyo-Ando K, Yamamoto A, Mitani S, and Arai H. (2010). Multivesicular body formation requires OSBP-related proteins and cholesterol. PLoS Genet 6.

Ma S, Henson ES, Chen Y, and Gibson SB (2016). Ferroptosis is induced following siramesine and lapatinib treatment of breast cancer cells. Cell Death Dis 7, e2307. [PubMed: 27441659]

Magtanong L, Ko P-J, To M, Cao JY, Forcina GC, Tarangelo A, Ward CC, Cho K, Patti GJ, Nomura DK, et al. (2019). Exogenous Monounsaturated Fatty Acids Promote a Ferroptosis-Resistant Cell State. Cell Chemical Biology 26, 420–432.e429.

Pan BT, T K, Wu C, Adam M, Johnstone RM. (1985). Electron microscopic evidence for externalization of the transferrin receptor in vesicular form in sheep reticulocytes. The Journal of cell biology 101, 942–948. [PubMed: 2993317]

Raposo G, and Stoorvogel W. (2013). Extracellular vesicles: exosomes, microvesicles, and friends. The Journal of cell biology 200, 373–383. [PubMed: 23420871]

Razi M FC (2006). Distinct roles for Tsg101 and Hrs in multivesicular body formation and inward vesiculation. Molecular biology of the cell 8, 3469–3483.

Saha SK, Islam SMR, Kwak K-S, Rahman MS, and Cho S-G (2019). PROM1 and PROM2 expression differentially modulates clinical prognosis of cancer: a multiomics analysis. Cancer Gene Therapy.

Shimada K, S R, Kaplan A, Yang WS, Hayano M, Dixon SJ, Brown LM, Valenzuela CA, Wolpaw AJ, Stockwell BR. (2016). Global survey of cell death mechanisms reveals metabolic regulation of ferroptosis. Nature chemical biology 12, 497–503. [PubMed: 27159577]

Singh RD, S A, Scheffer L, Holicky EL, Wheatley CL, Marks DL, Pagano RE. (2013). Prominin-2 expression increases protrusions, decreases caveolae and inhibits Cdc42 dependent fluid phase

endocytosis. Biochemical and biophysical research communications 434, 466–472. [PubMed: 23583380]

Stockwell BR, Friedmann Angeli JP, Bayir H, Bush AI, Conrad M, Dixon SJ, Fulda S, Gascón S, Hatzios SK, Kagan VE, et al. (2017). Ferroptosis: A Regulated Cell Death Nexus Linking Metabolism, Redox Biology, and Disease. Cell 171, 273–285. [PubMed: 28985560]

Torii S, Shintoku R, Kubota C, Yaegashi M, Torii R, Sasaki M, Suzuki T, Mori M, Yoshimoto Y, Takeuchi T, et al. (2016). An essential role for functional lysosomes in ferroptosis of cancer cells. The Biochemical journal 473, 769–777. [PubMed: 26759376]

Torti SV, M D, Paul BT, Blanchette-Farra N, Torti FM. (2018). Iron and Cancer. Annu Rev Nutr 21, 97–125.

Truman-Rosentsvit M, B D, Spektor L, Cohen LA, Belizowsky-Moshe S, Lifshitz L, Ma J, Li W, Kesselman E, Abutbul-Ionita I, Danino D, Gutierrez L, Li H, Li K, Lou H, Regoni M, Poli M, Glaser F, Rouault TA, Meyron-Holtz EG (2018). Ferritin is secreted via two distinct non-classical vesicular pathways. Blood 131, 342–352. [PubMed: 29074498]

Tsoi J, Robert L, Paraiso K, Galvan C, Sheu KM, Lay J, Wong DJL, Atefi M, Shirazi R, Wang X, et al. (2018). Multi-stage Differentiation Defines Melanoma Subtypes with Differential Vulnerability to Drug-Induced Iron-Dependent Oxidative Stress. Cancer cell 33, 890–904 e895. [PubMed: 29657129]

Viswanathan VS, R M, Dhruv HD, Gill S, Eichhoff OM, Seashore-Ludlow B, Kaffenberger SD, Eaton JK, Shimada K, Aguirre AJ, Viswanathan SR, Chattopadhyay S, Tamayo P, Yang WS, Rees MG, Chen S, Boskovic ZV, Javaid S, Huang C, Wu X, Tseng YY, Roider EM, Gao D, Cleary JM, Wolpin BM, Mesirov JP, Haber DA, Engelman JA, Boehm JS, Kotz JD, Hon CS, Chen Y, Hahn WC, Levesque MP, Doench JG, Berens ME, Shamji AF, Clemons PA, Stockwell BR, Schreiber SL (2017). Dependency of a therapy-resistant state of cancer cells on a lipid peroxidase pathway. Nature 547, 453–457. [PubMed: 28678785]

Weïwer M, B J, Lewis TA, Shimada K, Yang WS, MacPherson L, Dandapani S, Palmer M, Stockwell BR, Schreiber SL, Munoz B. (2012). Development of small-molecule probes that selectively kill cells induced to express mutant RAS. Bioorganic & medicinal chemistry letters 22, 1822–1826. [PubMed: 22297109]

Yang WS, Kim KJ, Gaschler MM, Patel M, Shchepinov MS, and Stockwell BR (2016). Peroxidation of polyunsaturated fatty acids by lipoxygenases drives ferroptosis. Proc Natl Acad Sci U S A 113, E4966–4975. [PubMed: 27506793]

Yang WS, SriRamaratnam R, Welsch ME, Shimada K, Skouta R, Viswanathan VS, Cheah JH, Clemons PA, Shamji AF, Clish CB, et al. (2014). Regulation of ferroptotic cancer cell death by GPX4. Cell 156, 317–331. [PubMed: 24439385]

Yang WS, and Stockwell BR (2008). Synthetic lethal screening identifies compounds activating iron-dependent, nonapoptotic cell death in oncogenic-RAS-harboring cancer cells. Chem Biol 15, 234–245. [PubMed: 18355723]

Yang WS, and Stockwell BR (2016). Ferroptosis: Death by Lipid Peroxidation. Trends in cell biology 26, 165–176. [PubMed: 26653790]

Zhang Y, Tan H, Daniels JD, Zandkarimi F, Liu H, Brown LM, Uchida K, O'Connor OA, and Stockwell BR (2019). Imidazole Ketone Erastin Induces Ferroptosis and Slows Tumor Growth in a Mouse Lymphoma Model. Cell Chem Biol 26, 623–633 e629. [PubMed: 30799221]

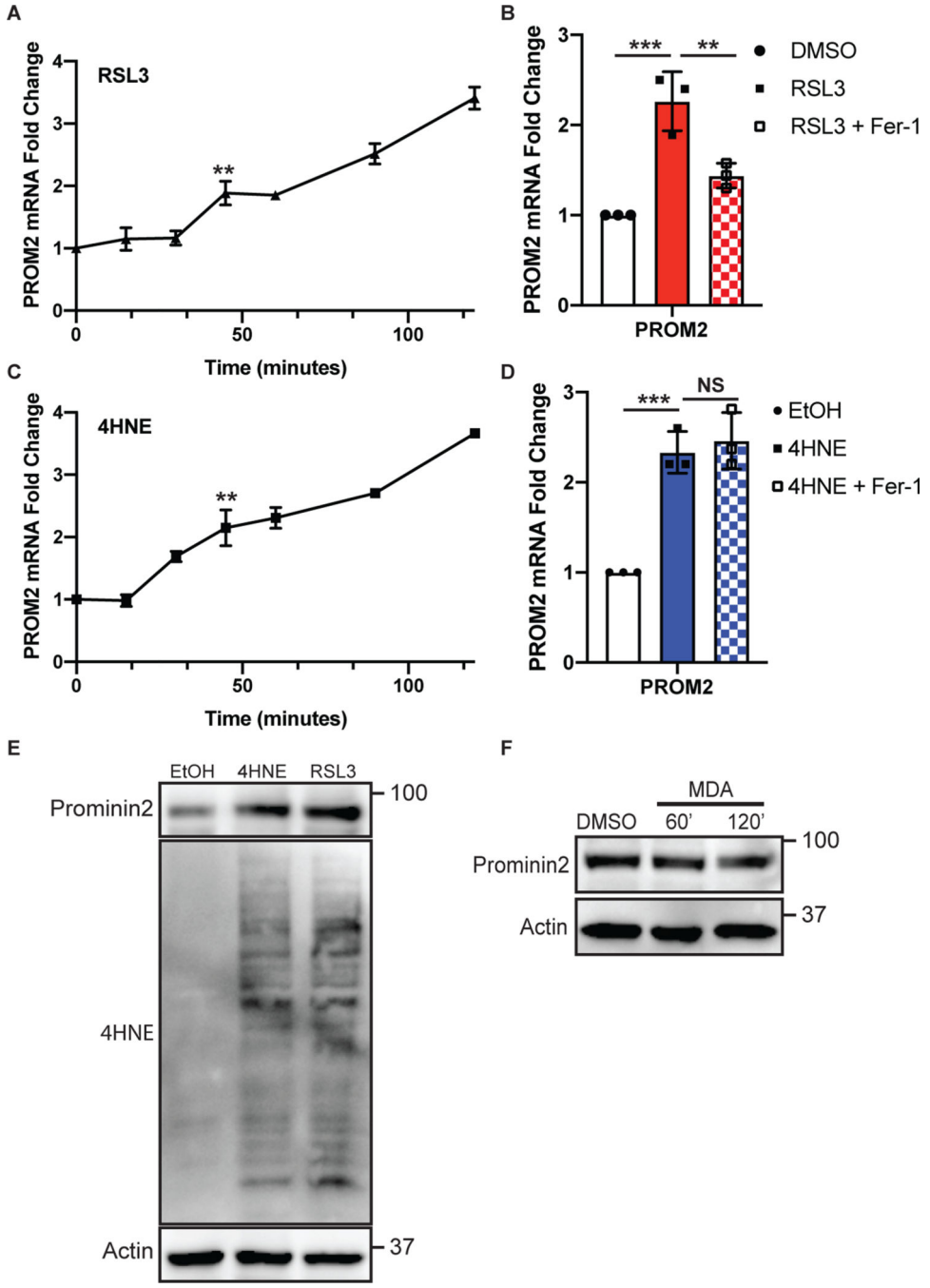

Figure 1. Prominin2 is a ferroptosis stress response protein.

(A) MCF10A cells were detached from ECM for 30 min, 1 hr, 2 hrs or 3 hrs. Extracts from these cells were immunoblotted for prominin2 and actin. Immunoblot is representative of three independent experiments. **(B)** MCF10A and Hs578t cells were transfected with either control siRNA or prominin2 siRNA for 48 hrs and then maintained under adherent or ECM-detached conditions for 2 hrs. PROM2 mRNA expression was quantified by qPCR. Shown is representative experiment of three independent replicates. **(C)** siControl or siProminin2-treated MCF10A and Hs578t cells were maintained in ECM detached conditions for 24 hrs

in the presence of either DMSO, ferrostatin-1 (2 μM), ZVAD-fmk (25 μM) or ferrostatin-1 and ZVAD-fmk and the number of viable cells was quantified. Shown is representative experiment of three independent replicates. **(D)** Adherent MCF10A, Hs578t and MDA-MB-231 cells were treated with either DMSO or RSL3 for 2 hrs and PROM2 mRNA expression was quantified by qPCR. Shown is representative experiment of three independent replicates. **(E)** Extracts from the cells in (**D**) were immunoblotted with antibodies specific for prominin2 and tubulin. The densitometric analysis of these immunoblots (normalized to 1.0 for each cell line) obtained from analysis of three independent experiments in shown below the blots. **(F)** Adherent MCF10A, Hs578t and MDA-MB-231 cells were treated with DMSO or RSL3 24 hrs and the percent of surviving cells was quantified. Absorbance was normalized to DMSO control. Shown is representative experiment of three independent replicates.

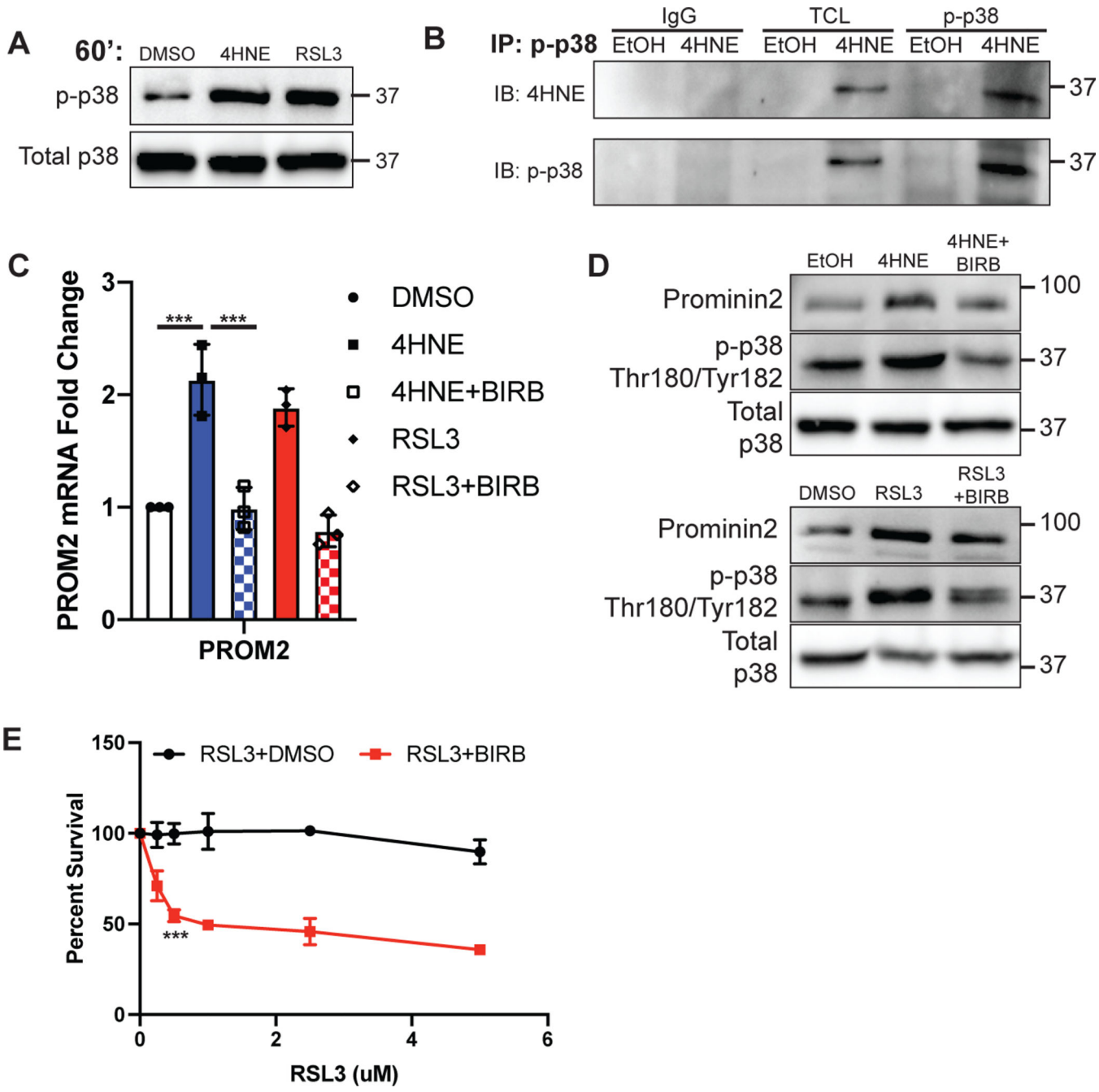

Figure 2. Prominin2 increases resistance to ferroptosis.

(A) Prominin2 expression was diminished in adherent MCF10A cells for 48 hours using siRNA prior to treatment with RSL3, ML210, FIN56 or erastin for for 24 hrs. The percent of surviving cells was quantified and compared to cells transfected with an siRNA control. Absorbance was normalized to DMSO control. Shown is representative experiment of three independent replicates. See Supplemental Information for the IC_{50} values for these conditions. **(B)** Prominin2 expression was diminished in adherent Hs578t cells for 48 hours using siRNA prior to treatment with RSL3, ML210, FIN56, or erastin for 24 hrs. The percent of surviving cells was quantified and compared to cells transfected with an siRNA

control. Absorbance was normalized to DMSO control. Shown is representative experiment of three independent replicates. See Supplemental Information for the IC_{50} values for these conditions. **(C)** Prominin2 expression was diminished in adherent MCF10A and Hs578t cells for 48 hours using siRNA. Cells were treated with either DMSO, RSL3 (5 μM) or RSL3 and ferrostatin-1 (2 μM) for 24 hrs and the percent of surviving cells was quantified. Shown is representative experiment of three independent replicates. **(D)** MDA-MB-231 cells were transfected with either a prominin2 expression construct or a vector control prior to treatment with either DMSO or RSL3 for 2 hrs. The percent of surviving cells was quantified. Absorbance was normalized to DMSO control. Shown is a representative experiment of three independent replicates.

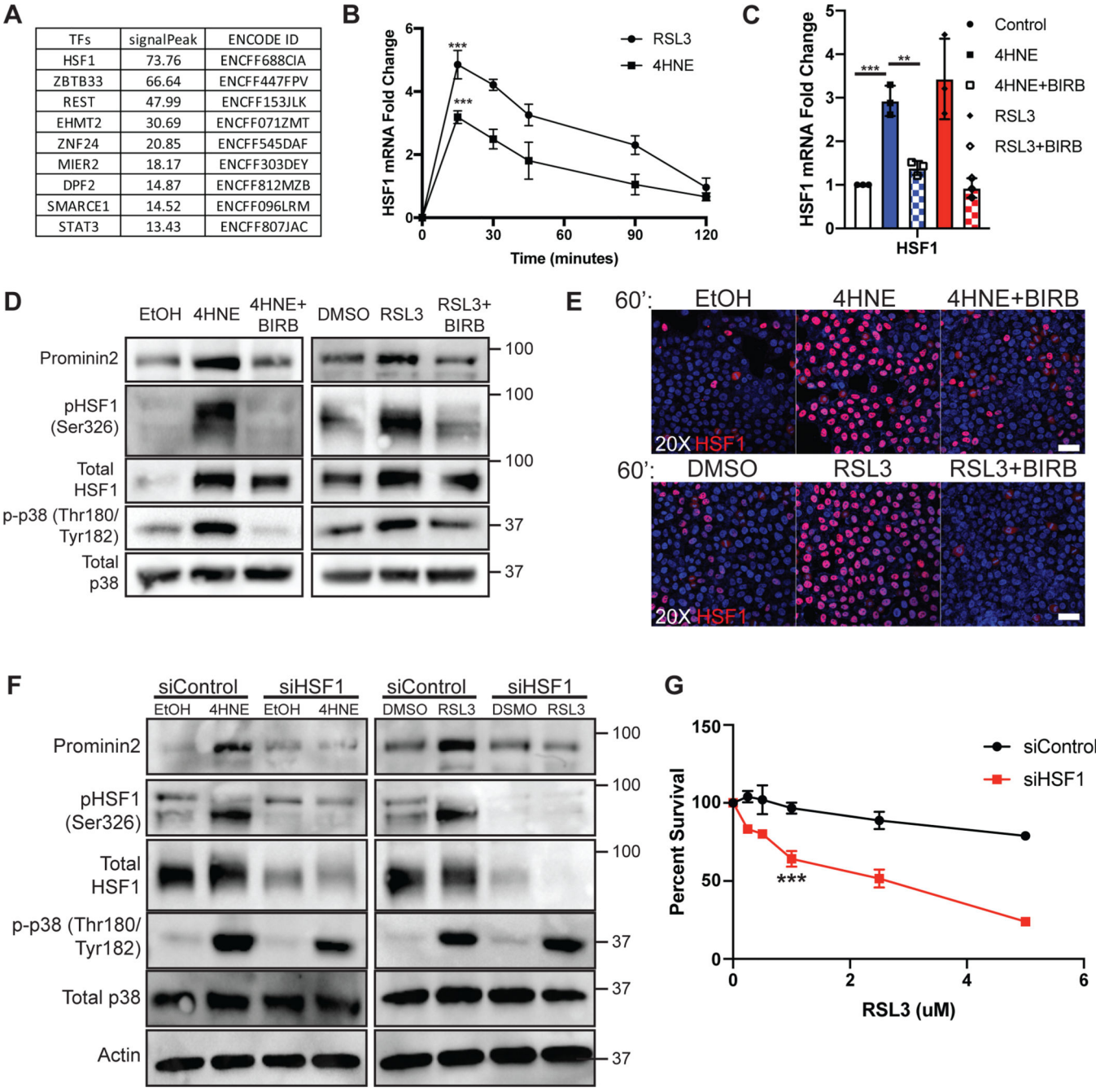

Figure 3. Prominin2 promotes the formation of multivesicular bodies (MVBs) in response to GPX4 inhibition.

(A) Adherent MCF10A and Hs578t cells were treated with either DMSO or RSL3 for 2 hrs and immunostained using Abs specific for TSG101 (green) and prominin2 (red). Scale bar = 10 μm. For all immunofluorescence images, merged images are shown in the main figures and single channel images are provided in Supplemental Information. Also, for all experiments, image acquisition settings were the same for DMSO and RSL3-treated cells. Shown is representative image of three independent replicates. **(B)** Adherent Hs578t cells were treated with either DMSO or RSL3 for either 1, 1.5 or 2 hrs and immunostained using

Abs specific for TSG101 (green) and prominin2 (red). Scale bar = 10 μm. Shown is representative image of three independent replicates. **(C)** MCF10A cells were transfected with either control siRNA or prominin2 siRNA for 48 hrs and then treated with either DMSO or RSL3 for 1.5 hrs. These cells were fixed and processed for transmission electron microscopy (TEM). The frequency of MVBs (white box) per section was quantified (right graph). Shown is representative image of five total cells quantified per group. **(D)** MCF10A cells and were transfected with either control siRNA or prominin2 siRNA for 48 hrs and then treated with either DMSO or RSL3 for 2 hrs. These cells were then immunostained using Abs specific for TSG101 (green) and prominin2 (red). Scale bar = 10 μm. Shown is representative image of three independent replicates. **(E)** Hs578t cells and were transfected with either control siRNA or prominin2 siRNA for 48 hrs and then treated with either DMSO or RSL3 for 2 hrs. These cells were then immunostained using Abs specific for TSG101 (green) and prominin2 (red). Scale bar = 10 μm. Shown is representative image of three independent replicates. **(F)** MDA-MB-231 cells were transfected with either a prominin2 expression construct or a vector control prior to treatment with either DMSO or RSL3 for 2 hrs. These cells were then immunostained using antibodies specific for TSG101 (green) and prominin2 (red). Scale bar = 10 μm. Shown is representative image of three independent replicates.

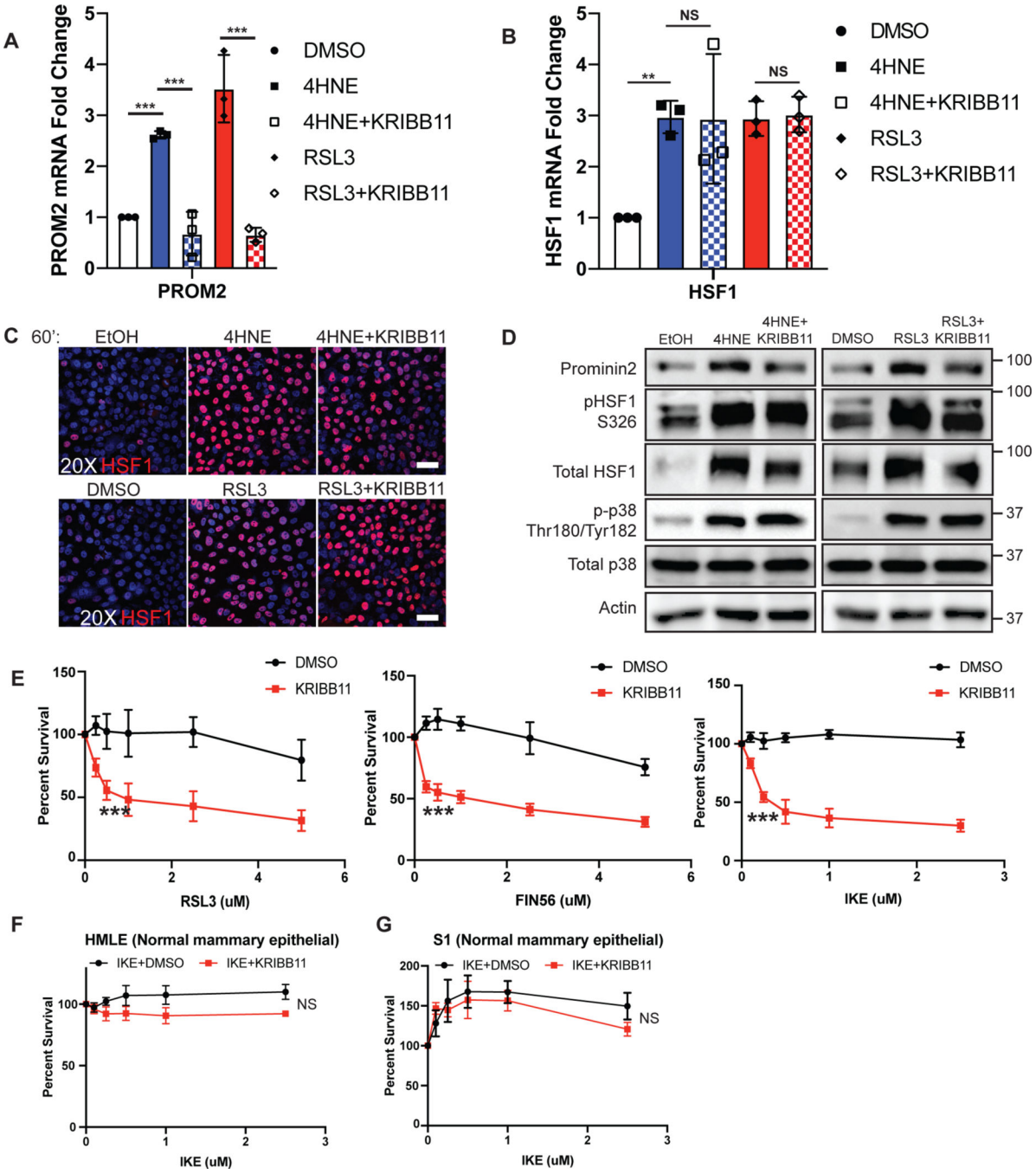

Figure 4. Multivesicular body formation is required for evasion of ferroptosis.

(A) TSG101 expression was diminished in adherent MCF10A cells for 48 hours using siRNA prior to treatment with DMSO or RSL3 for 24 hrs. The percent of surviving cells was quantified and compared to cells transfected with an siRNA control. Absorbance was normalized to DMSO control. Shown is representative experiment of three independent replicates. **(B)** TSG101 expression was diminished in adherent Hs578t cells for 48 hours using siRNA prior to treatment with DMSO or RSL3 for 24 hrs. The percent of surviving cells was quantified and compared to cells transfected with an siRNA control. Absorbance

was normalized to DMSO control. Shown is representative experiment of three independent replicates. **(C)** TSG101 expression was diminished in adherent MCF10A cells for 48 hours using siRNA prior to treatment with DMSO, RSL3 or RSL3 and ferrostatin-1 for 24 hrs. The percent of surviving cells was quantified and compared to cells transfected with an siRNA control. Absorbance was normalized to DMSO control. Shown is representative experiment of three independent replicates. **(D)** Exosomes were isolated from cell culture medium of MCF10A and Hs578t cells treated for 24 hours with 1 μM RSL3 by ultracentrifugation. The exosome pellets were lysed and protein concentration was assessed. Exosomes from RSL3 treated MCF10A and Hs578t cells were immunoblotted for TSG101, prominin2, GM130 and CD63. See Supplemental Information for TEM of exosomes. Shown is representative immunoblot of three independent collections. **(E)** Prominin2 expression was diminished in MCF10A and Hs578t cells for 48 hours using siRNA prior to treatment with either DMSO, RSL3 (5 μM) or RSL3 and the exosome inhibitor GW4869 (20 μM) for 24 hrs and the percent of surviving cells was quantified. Shown is representative experiment of three independent replicates.

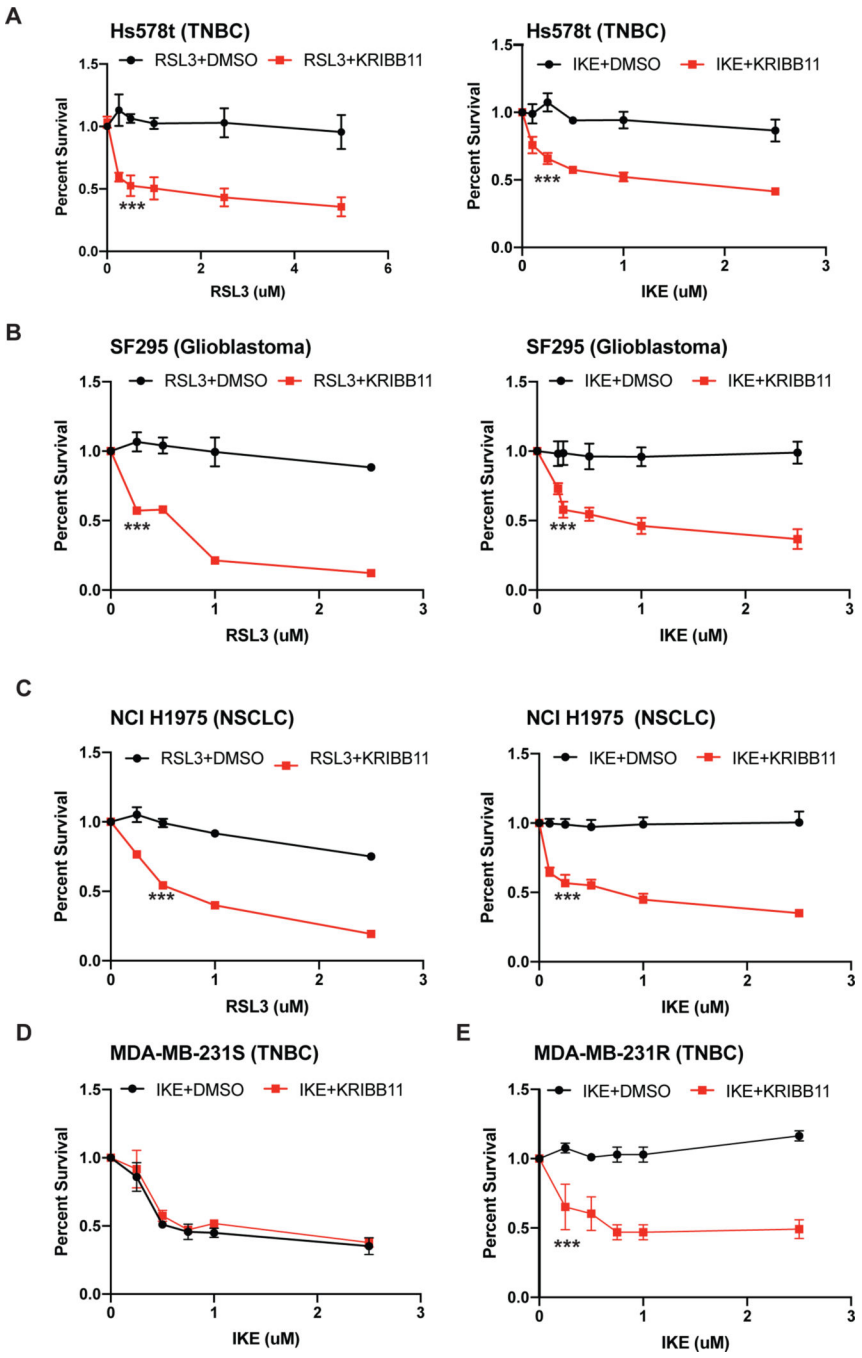

Figure 5. Prominin2 and ferritin contribute to the regulation of free iron.

(A) Adherent MCF10A and Hs578t cells were treated with either DMSO or RSL3 for 2 hrs and immunostained using Abs specific for ferritin (green) and prominin2 (red). Scale bar = 10 μm. Images are representative of three independent experiments with similar results. **(B)** Exosomes purified from RSL3-treated MCF10A and Hs578t cells as described in Fig. 3D were immunoblotted for prominin2, TSG101 and ferritin. **(C)** MDA-MB-231 cells were transfected with either a prominin2 expression construct or a vector control prior to treatment with either DMSO or RSL3 for 2 hrs. These cells were then immunostained using

antibodies specific for ferritin heavy chain (green) and prominin2 (red). Scale bar = 10 μm. Shown are representative images of three independent experiments. **(D)** MCF10A were transfected with either control siRNA or ferritin heavy chain siRNA for 48hrs and then treated with increasing concentrations of RSL3 for 24 hrs, and the percent of surviving cells was quantified. Shown is representative experiment of three independent replicates. **(E)** Hs578t cells were transfected with either control siRNA or ferritin heavy chain siRNA for 48 hrs and then treated with increasing concentrations of RSL3 for 24 hrs, and the percent of surviving cells was quantified. Shown is representative experiment of three independent replicates. **(F)** MCF10A and Hs578t cells were transfected with either control siRNA or ferritin siRNA for 48 hrs and then treated with increasing concentrations of either DMSO, RSL3 and ferrostatin-1, or RSL3 and deferoxamine (DFO) for 24 hrs. The percent of surviving cells was then quantified. Shown is a representative experiment of three independent replicates.

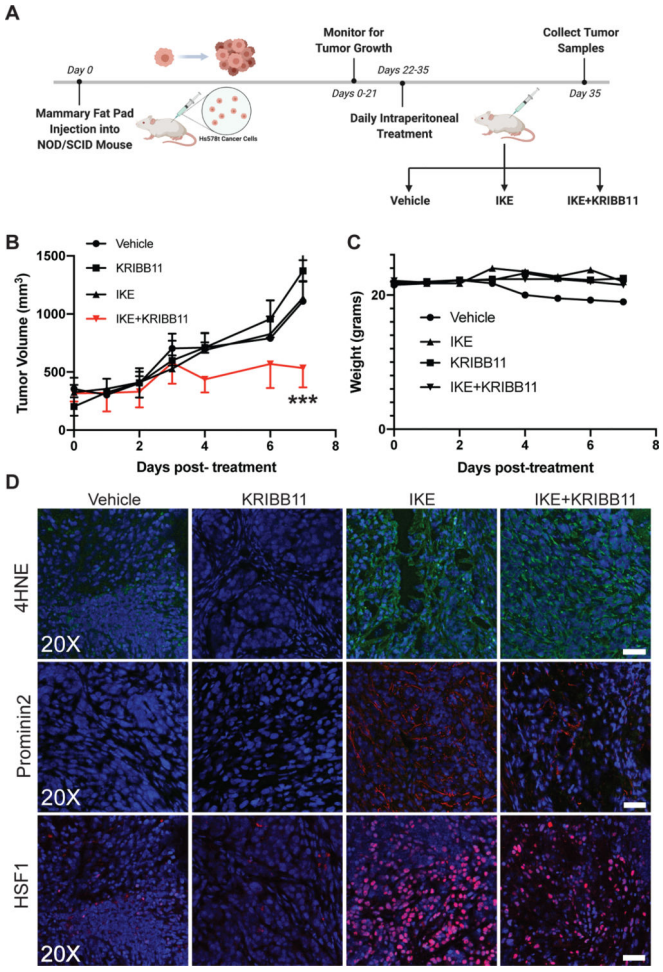

Figure 6. GPX4 inhibition alters free iron concentration.

(A) Adherent MCF10A and Hs578t cells were transfected with either control siRNA or prominin2 siRNA for 48 hrs and then treated with 5 μM RSL3 for 2 hrs. Total free iron was quantified and reported in nmols. Shown is a representative experiment of three independent replicates. **(B)** Adherent MCF10A and Hs578t cells were transfected with either control siRNA or ferritin heavy chain siRNA for 48 hrs and then treated with RSL3 for 2hrs. Total free iron was quantified and reported in nmols. Shown is a representative experiment of three independent replicates. **(C)** Adherent MDA-MB-231 cells were transfected with either a prominin2 expression construct or a vector control prior to treatment with either DMSO or RSL3 for 2 hrs. Total free iron was quantified and reported as nmols. Shown is representative experiment of three independent replicates. **(D)** Adherent MCF10A and Hs578t cells were transfected with either control siRNA or TSG101 siRNA for 48 hrs and then treated with either DMSO or RSL3 for 2 hrs. Total free iron was quantified and reported as nanomoles. Shown is representative experiment of three independent replicates.

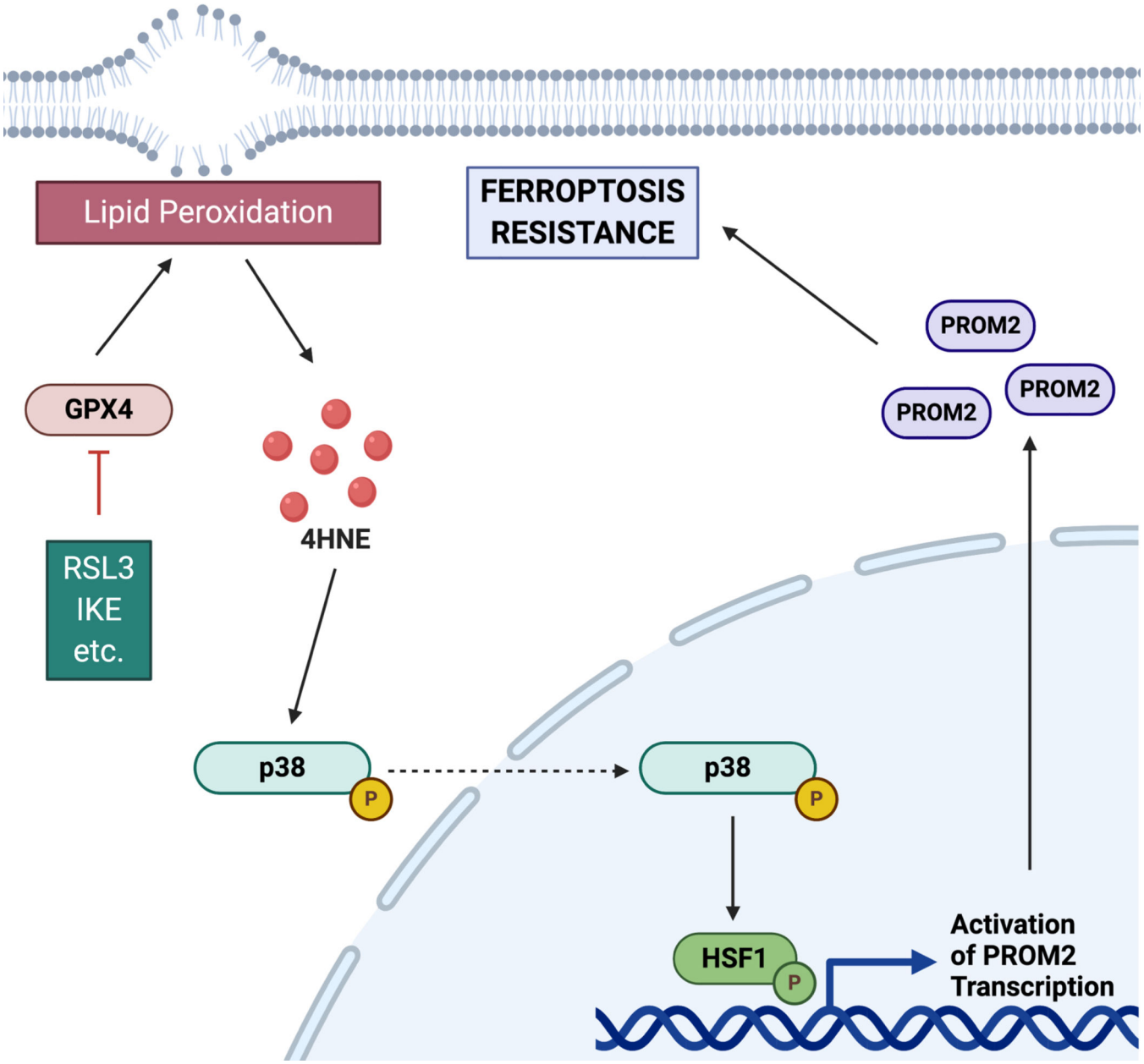

Figure 7. Detachment from the extracellular matrix induces prominin2-dependent MVB formation to rescue ferroptosis.

(A) Control and prominin2-depleted MCF10A cells were maintained in ECM-detached conditions for 24 hrs in the presence of either DMSO or deferoxamine and the number of viable cells was quantified. Shown is representative experiment of three independent replicates. **(B)** Control and prominin2-depleted MCF10A cells were maintained in ECM-detached conditions for the indicated times and total free iron was quantified. Shown is representative experiment of three independent replicates. **(C)** Control and prominin2-depleted MCF10A cells were maintained in ECM-detached conditions for 2 hrs and processed for TEM. The frequency of MVBs (white box) per section was quantified (right graph). Shown is representative image of five total cells quantified per group. **(D)** MCF10A

and Hs578t cells were maintained in ECM-detached conditions for 2 hrs, fixed and immunostained for TSG101 (green) and prominin2 (red). Scale bar = 10 μm. Shown are representative images of three independent experiments.

KEY RESOURCES TABLE

REAGENT or RESOURCE	SOURCE	IDENTIFIER
Antibodies		
Prominin2, rabbit polyclonal	Abcam	Cat#ab74977; Lot GR182311–23
Tubulin, mouse monoclonal	Sigma-Aldrich	Cat#T5168; Lot 038M4813V; RRID: AB_477579
TSG101, mouse monoclonal	Genetex	Cat#GTX70255; Clone: 4A10; Lot 43353; RRID: AB_373239
Ferritin Heavy Chain (FTH1), rabbit monoclonal	Thermo Fisher	Cat#701934; Lot 2010234; RRID: AB_2633038
Ferritin Light Chain (FTL), rabbit polyclonal	Abcam	Cat#ab69090; RRID: AB_1523609
Catalase, mouse monoclonal	Abcam	Cat#ab110292; Lot GR107615-C; RRID: AB_10859065
Phospho-Caveolin1, mouse monoclonal	Santa Cruz Biotechnology	Cat#sc-373837; RRID: AB_10988387
Rab5A, rabbit polyclonal	Santa Cruz Biotechnology	Cat#sc-46692; Clone D-11; Lot D0518; RRID: AB_628191
LC3, mouse monoclonal	MBL International	Cat#M152–3; RRID: AB_1279144
LAMP1, mouse monoclonal	R&D Systems	Cat#MAB4800; RRID: AB_10719137
A427:31lexa Fluor® 488 Goat anti-mouse	BioLegend	Cat#405319; RRID: AB_2563044
Alexa Fluor® 555 Donkey anti-rabbit	BioLegend	Cat#406412; RRID: AB_2563181
ALIX, mouse monoclonal	Abcam	Cat#ab117600; RRID: AB_10899268
NCOA4, mouse monoclonal	Sigma-Aldrich	Cat#SAB1404569–100UG; RRID: AB_10759525
Ferroportin/SLC40A1, mouse monoclonal	Novus Biologicals	Cat# NBP2–45357SS; RRID: AB_1215496
CD63, rabbit monoclonal	Abcam	Cat#ab217345; RRID: AB_2754982
Bacterial and Virus Strains		
Biological Samples		
Chemicals, Peptides, and Recombinant Proteins		
Mitotracker	Thermo Fisher	Cat#M7512
RSL3	SelleckChem	Cat#S8155
FIN56	SelleckChem	Cat#S8254
ML210	Sigma-Aldrich	Cat#SML0521
Erastin	SelleckChem	Cat#S7242
Ferrostatin-1	Sigma-Aldrich	Cat#SML0583
ZVAD-FMK	SelleckChem	Cat#S7023
GW4869	Sigma-Aldrich	Cat#D1692
Deferoxamine (DFO)	Sigma-Aldrich	Cat#D9533

REAGENT or RESOURCE	SOURCE	IDENTIFIER
Lipofectamine 3000	Thermo Fisher	Cat#L3000008
0.1% Triton	JT Baker	Cat#X198–05
Bovine Serum Albumin	MilliporeSigma	Cat#A7906
4% Paraformaldehyde	Boston Bioproducts	Cat#BM-155
RIPA Lysis Buffer	Boston Bioproducts	Cat#BP-115
Vectashield Antifade with DAPI	Vector Labs	Cat#H-1200
Crystal Violet	Fisher Scientific	Cat#C581
DMSO	Fisher Scientific	Cat#BP231
G418	Gibco	Cat#10131035
60mm Low Attachment Plates	S-Bio	Cat#MS-9035xz
Ammonium chloride	MilliporeSigma	Cat#A-0171
Critical Commercial Assays		
Iron Assay	Abcam	Cat#ab83366
Bradford Assay	Bio-Rad	Cat#5000006
Deposited Data		
MCF10A RNAseq	GEO	GSE115059
Experimental Models: Cell Lines		
Human Normal Mammary Epithelial, MCF10A	Barbara Ann Karmanos Cancer Institute	
Human Triple Negative Breast Carcinoma, Hs578T	Laboratory of Dr. Dohoon Kim (University of Massachusetts Medical School)	
Human Triple Negative Breast Carcinoma, MDA-MB-231	ATCC	Cat# HTB-26
Experimental Models: Organisms/Strains		
Escherichia coli competent cells	Promega	Cat#L2005
Oligonucleotides		
Custom *18s*	Forward 5'-AACCCGTTGAACCCCATT-3', Reverse 5'-CCATCCAATCGGTAGTAGCG-3'	N/A
Custom *PROM2*	Forward 5'- GCTCAGGAACCCAAACCTGT-3', Reverse 5'- GGCAGGCCATACATCCTTCT-3'	N/A
Custom *PROM1*	Forward 5'-AGTCGGAAACTGGCAGATAGC-3', Reverse 5'- GGTAGTGTTGTACTGGGCCAAT-3'	N/A
PROM2 siRNA	Santa Cruz Biotechnology	Cat#sc-94521
TSG101 siRNA	Santa Cruz Biotechnology	Cat#sc-36752
FTL siRNA	Santa Cruz Biotechnology	Cat#sc-40577
FTH1 siRNA	Santa Cruz Biotechnology	Cat#sc-40575
Recombinant DNA		
pRP[Exp]-EGFP/Neo-CMV>hPROM2[NM_001165978.2]	Vectorbuilder	N/A
Exosome Cyto-Tracer, pCT-CD63-GFP	System Biosciences	Cat#CYTO120-VA-1
Software and Algorithms		
GraphPad Prism	GraphPad Software	https://www.graphpad.com/scientific-software/prism/

REAGENT or RESOURCE	SOURCE	IDENTIFIER
Other		
DMEM High Glucose Media	Gibco	Cat#11965118
DMEM/F:12 Media	Gibco	Cat#11320082
8 well Chamber Slides	Mattek	Cat#CCS-8
Cholera Toxin	MilliporeSigma	Cat#C8052
EGF	Peprotech	Cat#AF-100–15
Hydrocortisone	MilliporeSigma	Cat#H4001
Insulin	MilliporeSigma	Cat#I5500
0.5 % Trypsin-EDTA (10x)	Gibco	Cat#15400–54